DEFORMATION MODES OF PACKINGS OF FRICTIONLESS POLYDISPERSE SPHERES

O. I. IMOLE, N. KUMAR, AND S. LUDING

Multi-Scale Mechanics, TS, CTW, University of Twente, P.O. Box 217, 7500 AE Enschede, NL
Email: o.i.imole@ctw.utwente.nl

Abstract

Dense granular materials are well known to demonstrate mechanical properties that are different from classical fluids or solids. An issue is the accurate prediction of mechanical properties of granular materials, which are controlled by the internal structure of the assembly of grains – where the internal structure itself depends on the history of the sample. In this work, the Discrete Element Method (DEM) approach is presented as a viable tool to investigate the behavior and dynamics of granular packings subjected to deformations. The results on uniaxial and deviatoric deformations are compared to earlier results on isotropic deformation. As main result, the evolution of pressure and coordination as a function of volume fraction are reported for both uniaxial and deviatoric deformation modes. Our findings compare astonishingly well with results for purely isotropic compression. The second stress response namely anisotropy, is present as the evolution of the deviatoric stress as a function of the deviatoric strain. Similar data can be measured from experiments with the true biaxial tester which is work-in-progress, and both deformation modes are especially simple to realize experimentally.

Key words: DEM, Uniaxial deformation, Deviatoric deformation, Deviatoric stress and strain

1. INTRODUCTION

Dense granular materials are generally complex systems which show unique material properties, different from classical fluids or solids. Complex phenomena like dilatancy, shear band formation, history dependence, jamming and yield stress among others have attracted significant scientific interest over the past decade. A full understanding of their flow and deformation behaviour still remains a challenging problem.

It has been shown by Luding and Perdahcioglu (2011) that isotropic and deviatoric deformation modes are pure modes, while the uniaxial deformation test derives from the superposition of an isotropic and a deviatoric test. On the other hand, the biaxial tests involve mixed stress- and strain-control instead of completely prescribed strains. In this work, various deformations of polydisperse packings of non-frictional particles were modeled with the DEM approach. The evolution of coordination number, fraction of rattlers, isotropic fabric, and pressure (isotropic stress) are reported as function of volume fraction and isotropic strain, while the deviatoric stress is studied as function of the deviatoric strain, for different contact properties and system parameters. Some of these results are presented, while the comparison with experiments will be the focus of a future publication.

2. SIMULATION PROCEDURE

The Discrete Element Method (DEM) (Cundall and Strack 1979) was used to perform simulations in a tri-axial box. One advantage of the tri-axial box is the possibility of realizing different deformation modes with a single test experiment (element test) with a direct control of stress and strain (Luding and Perdahcioglu 2011, Tykhoniuk et al 2007). In addition, laboratory experiments with the triaxial box are also feasible in addition to many other (shear) testers (Roeck et al 2008, Tykhoniuk et al 2007). For initial simplicity, the contact model used in this work is the linear visco-elastic normal force

$$f^n = k\delta + \gamma\dot{\delta} \qquad\qquad (1)$$

where k is the spring stiffness, γ the contact viscosity parameter, δ the overlap between particle contacts and $\dot{\delta}$ is the relative velocity in the normal direction. Eq. (1) above determines the particle contact forces in the normal direction. In order to reduce dynamical effects and shorten relaxation times, an artificial viscous background dissipation force $f_b = -\gamma_b v_i$ proportional to the moving particle i with velocity v_i is added, resembling the damping due to a background medium.

3.1 Simulation parameters

Simulation parameters are: system size $N = 4913$ particles, density $\rho = 2000$ [kg/m^3], elastic stiffness $k_n = 10^5$ [kg/s^2], particle damping coefficient $\gamma = 1$ [kg/s], background dissipation $\gamma_b = 0.1$ [kg/s]. The work of Luding et al (2008) provides a description of these artificial units and how they can be rescaled to fit values obtained from experiments due to the simplicity of the contact model used. It should also be noted that the system has average particles radius $<r> = 1$ [mm], with polydispersity quantified by the width $w = r_{max}/r_{min} = 3$ of a uniform distribution defined in Göncü et al (2011) where r_{max} and r_{min} are the radius of the biggest and smallest particles respectively.

3.2 Initial configuration

(a) Uniaxial

The initial configuration is such that particles were randomly generated in a 3D box and isotropically compressed to a target volume fraction of $v_0 = 0.673$ above the jamming volume fraction. The isotropic compression stage is taken as the conditioning or preparation stage before the initiation of the test. Uniaxial compression is subsequently initiated at this point after allowing sufficient relaxation of the isotropic system. The volume fraction increases with time during compression to a maximum of $v_{max} = 0.82$ and back to the original v_0 (Fig. 2a).

Above the jamming volume fraction, contacts between the particles are deformed more and more with ongoing compression. The potential energy is an indicator of the overlap between particles hence its values are considerably larger than the kinetic energy (above jamming, see Fig. 2(b)). The ratio of the kinetic energy values to the potential energy values gives a rough indication that the system is above the jamming regime in the quasi-static state. Lower energy ratios can be obtained by performing slower rate simulations as seen in Fig. 2(b).

(b) Deviatoric

The initial configuration for the deviatoric deformations is such that particle configurations are taken from the isotropic un-loading branch below the maximum volume fraction. The deviatoric deformation mode is described by a three-dimensional strain matrix that has non-zero elements on the diagonal, $\frac{1}{2}\varepsilon_D(-\frac{1}{2}, -\frac{1}{2}, 1)$. One wall moves twice as much inwards as the other two walls move outwards such that volume is conserved during deformation and relaxation.
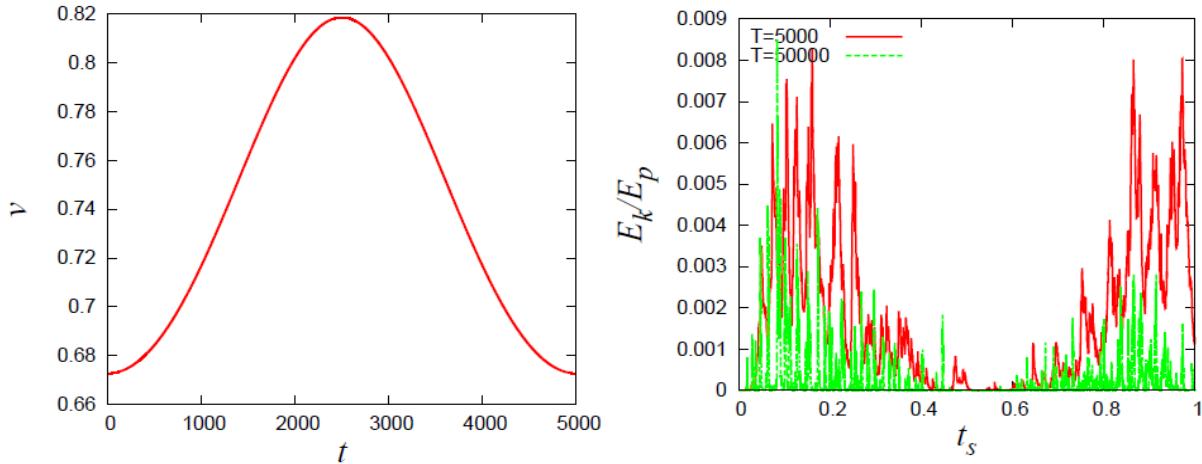

Fig. 2(a): Evolution of volume fraction as a function of time (t) for isotropic compression. Fig. 2(b): Comparison of ratio of kinetic energy to the potential energy in scaled time ($t_s = t/T$) for two uniaxial compression simulations where T is the period of one compression-decompression cycle ($E_k/E_p < 0.1$ percent). The simulation represented by the green curve is 10 times slower than the red.

3.3 Evolution of Coordination Number

Jamming occurs at the isostatic point (Göncü et al (2011), O'Hern et al (2002, 2003), Silbert, et al (2002)). The definition of an isostatic packing excludes all particles that do not contribute to the force network, i.e. particles with exactly zero contacts are excluded. In addition to the particles with zero contacts, there may be particles with some finite number of contacts, for some short time, which also do not contribute to the

mechanical stability of the packing. The contacts of these dynamic rattlers are transient because the repulsive contact forces will push them away from the mechanically stable backbone (Göncü et al (2011)). We define frictionless particles with less than 4 contacts as rattlers since they do not contribute to the force chain network and are not mechanically stable. In this work, rattlers have been identified by counting the number of contacts each particle makes with its neighbours. This leads to the following abbreviations and definitions:

N	:	Total Number of particles
$N_4 := N_{C \geq 4}$	:	Number of particles with at least 4 contacts
M	:	Total Number of Contacts
$M_4 := M_{C \geq 4}$	:	Number of contacts of particles with at least 4 contacts
$C^r := \frac{M}{N}$	:	Coordination number (classical definition)
$C = C^m := \frac{M_4}{N}$	:	Coordination number (modified definition)
$C^* := \frac{M_4}{N_4}$	:	Corrected Coordination number

The values of contact number originating from particles with $C=1$, 2 or 3 is so small as compared to those with $C=0$ that it is not astonishing that C^r and C^m are very similar. For our uniaxial simulations, the number fractions of the rattlers grow from about 2 percent at the beginning of the compression to a maximum of about 10 percent at the end of the compression cycle. For the deviatoric simulations, the number fraction of rattlers remains fairly constant since volume is conserved anyway. As expected, the ratio of M_4 and N_4 (the corrected coordination number) is slightly larger.
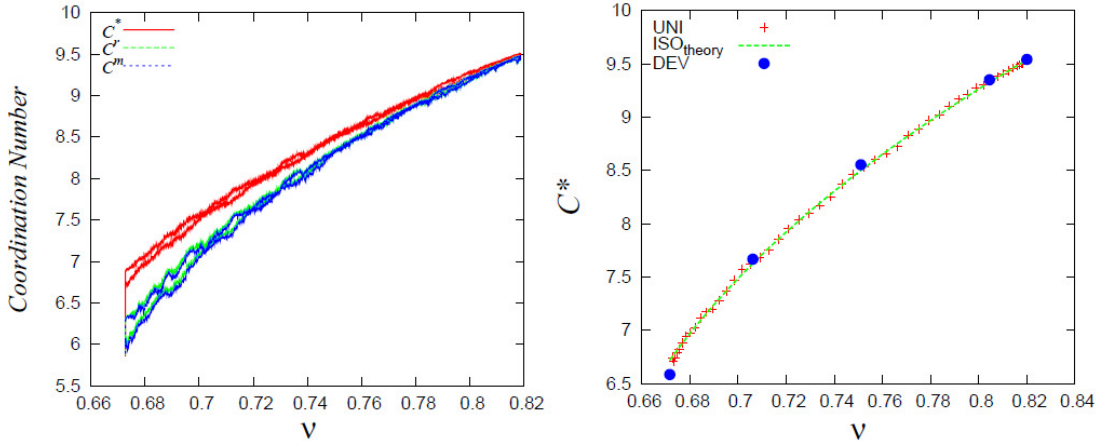

Fig. 3(a): Evolution of differently defined coordination numbers (C^* (red), C^r (green) and C^m (blue)) plotted against volume fraction for isotropic compression. Fig. 3(b): Comparison of (C^*) with the numerical data (red) and the proposed fit (green) Eq. (2). The blue dots represent the asymptotic values of coordination numbers for various different volume fractions after deviatoric deformation modes.

The plots of variation of C^*, C^r and C^m can be seen in Fig. 3(a). We have observed that C^* follows a power law with volume fraction

$$C^*(v) := C_0 + C_1 \left(\frac{v}{v_c} - 1 \right)^\alpha \tag{2}$$

where $C_0 \approx 3.921, C_1 \approx 9.658$ and $\alpha \approx 0.446$ are the fitted parameters to C^* vs v plot (Fig. 3(b)) above the jamming volume fraction $v_c \approx 0.665$. From this fit one can get the critical jamming volume fraction estimate too. One interesting thing to observe is that the data for the deviatoric deformation shown in Fig. 3(b) which is taken at the end of deviatoric simulations with different initial volume fractsions (since volume is conserved under pure shear deformation) also collapse on the curves representing the isotropic and uniaxial deformation. This suggests that for our simulations, the coordination number evolution equation proposed by (Göncü et al (2011)) in Eq. (2) above is independent of the deformation mode, when the particles are frictionless. For frictional systems, this observation might not hold.

3.4 Evolution of pressure under isotropic deformation

In this section, the relation between pressure and volume fraction is studied. The non-dimensional pressure (Göncü et al (2011)) is defined as:

$$p = \frac{2\langle r \rangle}{3k_n} tr(\sigma) \tag{3}$$

where $tr(\sigma)$ is the trace of the averaged stress tensor. The normalized average overlap $\langle \Delta \rangle_c = \delta_c / \langle r \rangle$ is related to the volumetric strain under the simplifying assumption of uniform deformation in the packing as:

$$d\langle \Delta \rangle_c = D\epsilon_v \tag{4}$$

where $\epsilon_v = \epsilon_{ii}$ is the trace of the infinitesimal strain tensor and D is a proportionality constant that depends on the size distribution. The integral of ϵ_v, denoted by ε_v is the true logarithmic volume change of the system relative to the reference volume V_0, with corresponding reference volume fraction, v_0 which is chosen without loss of generality to be equal to the critical, jamming volume fraction $v_0 = v_c$, so that the average normalized overlap:

$$\langle \Delta \rangle_c = D \int_{V_0}^{V} \epsilon_v = D\varepsilon_v = D\ln\frac{v_c}{v} \tag{5}$$

The non-dimensional pressure – strain (isotropic) relation is (Göncü et al (2011)):

$$p = p_0 \frac{vC}{v_c}(-\varepsilon_v)\big[1 - \gamma_p(-\varepsilon_v)\big] \tag{6}$$

and the scaled pressure is given as:

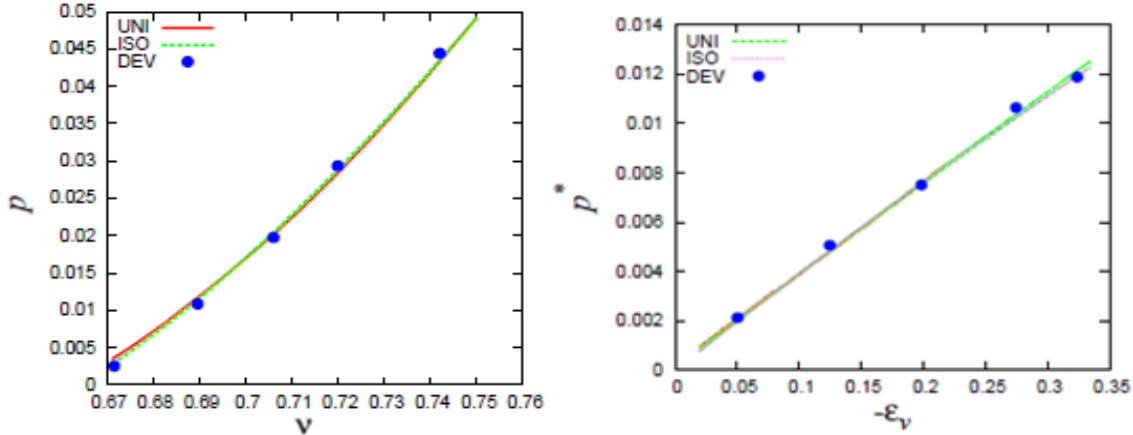$$p^* = \frac{pv_c}{vC} = p_0(-\varepsilon_v)\big[1 - \gamma_p(-\varepsilon_v)\big] \tag{7}$$

Fig. 4(a). Total non-dimensional pressure as a function of the volume fraction for the UNIaxial, ISOtropic and DEViatoric deformation Fig. 4(b). The scaled pressure as a function of the (negative) volumetric strain for the unloading cycle for an isotropic test (Göncü et al 2011) and the same data in (a).

Fig. 4(a) shows the total pressure (non-dimensional) as a function of the volume fraction for the Uniaxial, Isotropic and Deviatoric deformation. As stated earlier, volume is conserved in the Deviatoric deformation mode so that the data points (blue) shown in Fig 4(a) are taken from the end of simulation with different initial volume fractions. They also almost collapse on the plots for the two other deformation modes with slight deviations from of the deviatoric case possibly due to dilatancy or small dynamic effects as will be discussed further in Imole et al (2011). The isotropic data sets have been reported in Göncü et al (2011). Fig 4(b) shows the scaled pressure as a function of the (negative) volumetric strain with v_c=0.665 for a comparable isotropic compression data set and the uniaxial compression set being studied. Astonishingly, analytical prediction of the scaled pressure as a function of volumetric strain for an isotropic system compares well with our uniaxial simulation where the particles are frictionless. Other deformation rates studied collapse with the same curve for small deformations. The scaled pressure is also well represented by the linear relation $p^* \approx -p_0\varepsilon_v$ in Eq. (6) for small deformations. For all cases (isotropic, uniaxial and deviatoric), the coefficients $p_0 \approx 0.039$, $\gamma_p \approx 0.011$ and $v_c \approx 0.665$ fit our data well with errors of less than one percent for all densities. The deviatoric mode pressure data are off by 1-2% only.

4

3.5 Deviatoric stress

The average isotropic stress (pressure) is defined as:

$$p = \frac{\sigma_{xx} + \sigma_{yy} + \sigma_{zz}}{3} = \frac{1}{3} tr(\sigma) \tag{8}$$

The deviatoric stress and strain between the moving boundary (wall with normal in z-direction) and the two other periodic boundary walls (x and y) is defined by:

$$\sigma_{DEV1} = \sigma_{zz} - \frac{\sigma_{xx} + \sigma_{yy}}{2}; \quad \varepsilon_{DEV1} = \begin{cases} \varepsilon_{zz} \text{ for UNI} \\ \varepsilon_D \text{ for DEV} \end{cases} \tag{9}$$

Also, we define the second deviatoric stress, σ_{DEV2} and deviatoric strain ε_{DEV2} between the periodic boundary directions x and y in the system as:

$$\sigma_{DEV2} = \frac{\sigma_{xx} - \sigma_{yy}}{2}; \quad \varepsilon_{DEV2} = 0 \text{ for UNI and DEV} \tag{10}$$

The first deviatoric stress (σ_{DEV1}) quantifies the (stress) anisotropy between the compression/de-compression direction and the non-deformed direction, while the second deviatoric stress (σ_{DEV2}) quantifies the anisotropy between the two equivalent non-deformed directions-which should be small for symmetry reasons. Fig. 5 shows the evolution of the deviatoric stress during loading and unloading. In order to compare the magnitude of σ_{DEV1} and σ_{DEV2} we normalize them with the isotropic pressure p and plot them as a function of the compression strain ε_{zz} in Fig. 5(a).
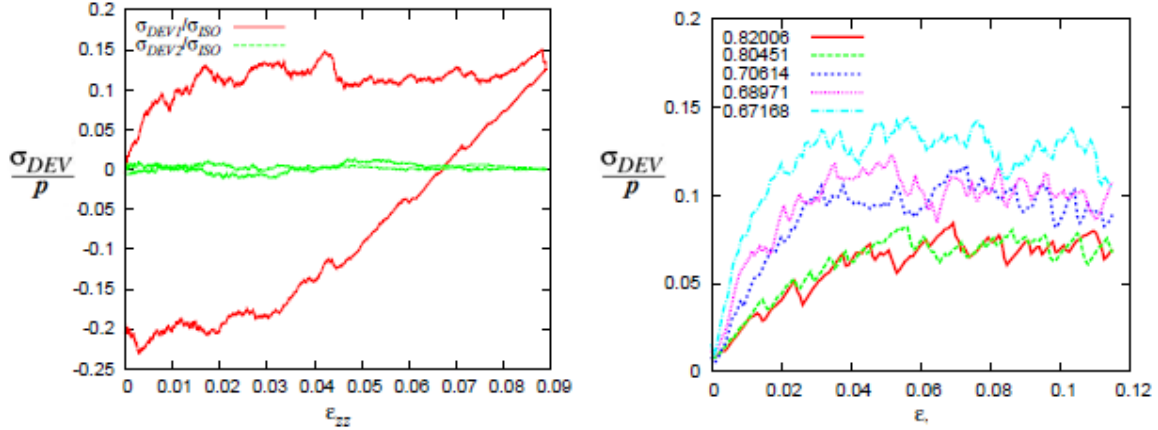

Fig. 5(a). Evolution of the deviatoric stress as a function of total strain for UNIaxial deformation. Fig. 4(b). Evolution of the deviatoric stress as a function of total strain for DEViatoric deformation for five different volume fractions.

The second deviatoric stress variation between the fixed periodic walls in the *x* and *y* plane lies close to zero during the loading and unloading cycles reflecting the symmetry in *x-y*-directions. In contrast, σ_{DEV1} shows some interesting profile. The stress increases up to ≈ 0.12 (12 ± 2 percent) from the commencement of the loading cycle and thereafter remains fairly constant till the end of the loading cycle. During unloading, it decreases almost linearly until it gets to the isotropic state ($\frac{\sigma_{DEV}}{p} = 0$) and goes to ≈ -0.2 (-20 ± 2 percent) relative to the start-up point. Interestingly, the initial zero deviatoric stress at strain $\varepsilon_{zz} \approx 0.066$ is not recovered when the initial value of volume fraction is reached. This means the system stays anisotropic after the complete cyclic path, visible as a hysteretic loop, indicating history (memory) effects.

The loading response for our deviatoric simulations is shown in Fig 5(b) and is similar to the UNI loading branch, but here we have five different normalized shear stresses for different initial volume fractions. For each volume fraction, stresses evolve linearly until an asymptote is reached, where the values stays almost constant. Systems with higher volume fractions have smaller normalized stress values.

4. CONCLUSION

We have presented simulation results from the strain controlled uniaxial compression and deviatoric deformation of frictionless polydisperse spheres as far as coordination number and pressure are concerned. An important result in this study is the agreement obtained for the analytical predictions of the scaled pressure as function of volumetric strain for a purely isotropic system and our simulations with different deformation modes. It is also interesting that the asymptotic values (after large deviatoric strain applied) of the pressure for

different volume fractions all collapse on the uniaxial and purely isotropic data set. This tells us that the deformation mode is not significant during the deformation of frictionless polydisperse spheres. This suggests an advantage of the 'cheaper' uniaxial and deviatoric deformation experimental setup over isotropic deformation. Three walls have to be moved simultaneously in the isotropic case while less movement is required in the other modes. The second observation is the confirmation of symmetry in the two non-mobile directions, and the observation of particular stress anisotropy evolution for the uniaxial case, as similar to the deviatoric case

For further work, more realistic contact models to incorporate friction and cohesion need to be implemented and physical experiments on cohesive powders with the bi-axial box needs to be performed and compared. The theory for different deformation modes (Luding et al 2011) also need to be fine-tuned.

6. ACKNOWLEDGEMENT

7. REFERENCES

Cundall P.A., Strack, O.D.L., A discrete numerical model for granular assemblies. In Geotechnique, vol. 29, pp. 47-65, 1979.

Göncü, F., O. Duran, and S. Luding, Constitutive relations for the isotropic deformation of frictionless packings of polydisperse spheres, C. R. Mecanique 338, 570-586, 2010.

Kruyt, N. P., "Three-dimensional lattice-based dispersion relations for granular materials," in IUTAM-ISIMM Symposium on Mathematical Modeling and Physical Instances of Granular Flows (J. Goddard, P. Giovine, and J. T. Jenkins, eds.), (Reggio Calabria (Italy), 14.18 September 2009), pp. 405–415, AIP, 2010.

Luding S., Bauer E., "Evolution of swelling pressure of cohesive-frictional, rough and elasto-plastic granulates," in Geomechanics and Geotechnics: From Micro to Macro, (IS-Shanghai Conference Proceedings, 10.-12. Oct. 2010).

Luding, S., "Cohesive, frictional powders: contact models for tension," Granular matter, vol. 10, no. 4, 2008.

Luding, S., and S. Perdahcioglu, A local constitutive model with anisotropy for various homogeneous 2D Biaxial deformation modes, CIT 83(5), 672-688, 2011.

O'Hern, C. S., Langer S. A., Liu A. J., and Nagel S. R., "Random packings of frictionless particles," Phys. Rev. Lett., vol. 88, no. 7, 2002.

O'Hern, C. S., Silbert L. E., Liu A. J., and Nagel S. R., "Jamming at zero temperature and zero applied stress: The epitome of disorder," Phys. Rev. E, vol. 68, no. 1, Part 1, 2003.

Roeck M.; Morgeneyer M., Schwedes J., Brendel L., Wolf D. E., Kadau D.: Visualization of Shear Motions of Cohesive Powders in the True Biaxial Shear Tester. Volume 26, Issue 1, Pages 43 – 54, 2008.

Silbert, L. E., Ertas D., Grest G. S., Halsey T. C., and Levine D., "Geometry of frictionless and frictional sphere packings," Phys. Rev. E, vol. 65, p. 051302, Mar. 2002.

Tykhoniuk R., Tomas J., Luding S., Kappl M., Heim L., Hans-Jürgen Butt. Chem. Eng. Sci. Volume 62, Issue 11, Pages 2843-2864, June 2007.

Imole O.I., Kumar N., Magnanimo V., Luding S., Deformation modes of frictionless polydisperse spheres (in preparation)